Geochimica et Cosmochimica Acta, Vol. 69, No. 20, pp. 4919–4934, 2005

0016-7037/05 $30.00 + .00

doi:10.1016/j.gca.2005.05.017

Volcanism in Mare Fecunditatis and Mare Crisium: Ar-Ar age studies

VERA A. FERNANDES*,† and RAY BURGESS
Department of Earth Sciences, University of Manchester, Oxford Road, Manchester, M13 9PL, UK

(*Received July* 16, 2004; *accepted in revised form May* 16, 2005)

Abstract—The laser $^{40}Ar/^{39}Ar$ dating technique has been applied to five Luna 16 basalt fragments and one impact glass, and nine Luna 24 basalt fragments and one breccia. The textures of these basalts are fine-grained ophitic and coarse-grained basalts. The samples contain high levels of solar and lunar atmospheric argon acquired during their residence on the lunar surface. These trapped argon components are predominantly released at low temperature steps and can be distinguished from radiogenic and cosmogenic released at intermediate and high temperature steps. The apparent ages obtained for Luna 16 samples span a narrow range of 3.29 to 3.38 Ga. A young age of 0.988 Ga was obtained for a basaltic impact glass indicating the age of an impact event in the vicinity of Luna 16 landing site. The ages obtained for Luna 24 samples suggest the existence of at least three periods of volcanism occurring over a protracted interval of between 3.45 and 2.52 Ga. The long period of volcanism suggested for the Mare Crisium was likely due to a combination of geophysical and geochemical features in the surrounding and underlying areas of the Crisium Basin. Attempts at dating three Luna 20 samples were inconclusive due to their high trapped argon contents. *Copyright © 2005 Elsevier Ltd*

1. INTRODUCTION

Six American Apollo missions and three Soviet Luna missions brought ~380 kg of lunar samples for laboratory study. Materials from these missions, plus the subsequent lunar meteorite findings, have allowed scientists to take the first steps to construct a detailed geological history and evolution of the Moon. The few older rocks dated >4.2 Ga are cumulates of anorthosite and Mg-suite rocks and most have experienced a complex history. An age range for the eruption of lunar mare basalts of 3.9 to 3.1 Ga has been determined by different isotopic methods (summarized by Dalrymple, 1991; Papike et al., 1998; Stöffler and Ryder, 2001). Photogeologic evidence suggests that there were periods of volcanism occurring prior to the formation of the major nearside lunar basins (Schultz and Spudis, 1983; Bell and Hawke, 1984; Hawke et al., 1990; Head and Wilson, 1992; Head et al., 1997), which may have occurred as early as 4.2 Ga. The ages of lava flows younger than 3.1 Ga were first suggested after photogeologic observations by Schaber (1973), Schultz and Spudis (1983), Hiesinger et al. (2000), and Hiesinger and Head (2003) and more recently determined by Ar-Ar dating of Luna 24 samples (Burgess and Turner, 1998) and basaltic lunar meteorites (Fernandes et al., 2003; Borg et al., 2004).

The Luna 16 (1970) landing site is in the northeastern part of the Mare Fecunditatis in an area not affected by cratering ejecta (Vinogradov, 1971), but between the Langrenus and Taruntius craters (McCauley and Scott, 1972) of Eratosthenian and Copernican ages respectively. This mare is within Fecunditatis Basin, one of the most degraded multi-ringed basins on the Moon (McCauley and Scott, 1972). The robotic mission drilled to a depth of 35 cm and collected ~100 g of material from the upper regolith layer. Most of the fragments obtained were basaltic (Vinogradov, 1971) with an aluminous (~13 wt.% Al_2O_3), low Ti (~5 wt.% TiO_2) chemical composition (Ma and Schmitt, 1979). Until recently, the age of only three fragments had been determined; this number has now been increased to 13 by Cohen et al. (2001) and the present study. The dominant age found for mare fragments obtained at this site is ~3.4 Ga (Huneke et al., 1972; Cadogan and Turner, 1977; Cohen et al., 2001).

The Luna 20 mission (1972) was the second unmanned Soviet mission and the only one to collect a regolith core from the eastern highlands of the lunar nearside. The Luna 20 landing site is 120 km north of the Luna 16 landing site (Vinogradov, 1973) located on the hillside of Crisium Basin beyond the rings flooded with mare lavas, and considered to be inside a buried portion of the main rim (Wilhelms, 1987). Apollonius C crater (Copernican) is located several kilometers from the Luna 20 site, and Vinogradov (1973) suggested that its ejecta might constitute much of the Luna 20 material. A total of ~50 g of material was collected with the main component being anorthositic rocks (ANT), with minor components of basaltic rocks and impact melts (Swindle et al., 1991). The age range of 3.75 to 4.5 Ga (Cadogan and Turner, 1977; Podosek et al., 1973; Swindle et al., 1991) obtained for Luna 20 fragments indicate that these fragments are from old crust and also that this region experienced a significant input from impact events as evidenced by the re-setting of the Ar-Ar ages of these samples. Previously, the ages of samples from Luna 20 have been used to constrain the time of Crisium Basin formation (Cadogan and Turner, 1977), however Podosek et al. (1973) have suggested that some material from the Fecunditatis and Tranquilitatis Basins is also present.

Luna 24 (1976) was the third unmanned Soviet mission and the last time samples were ever purposely obtained from the lunar surface. The Luna 24 landing site is located on the southeastern region of Mare Crisium on the inner mare surface. A core of lunar regolith was drilled with a mass of ~170 g. The

* Author to whom correspondence should be addressed (veraafernandes@yahoo.com).
† *Present address:* Inst. Geofísico, Univ. Coimbra, Av. Dr. Dias da Silva, Coimbra, Portugal.

Table 1. Summary of sample preparation procedures and analytical methods performed on each fragment.

Sample	Split	SEM	EMPA	Ar-Ar
21000,20-A	✓	✓	X	✓
21000,20-B	✓	✓	✓	✓
21000,20-C	X	X	X	X
21000,20-D	✓	✓	✓	✓
21013,51-B Spherule	✓	✓	✓	✓
21013,51-D	✓	✓	✓	✓
21013,51-E	✓	✓	X	✓
24077,92-A	✓	✓	✓	✓
24077,92-B	✓	✓	✓	✓
24077,92-C	X	X	X	✓
24077,92-D	X	X	X	✓
24077,92-E	X	X	X	✓
24109,92-A	✓	✓	✓	✓
24109,92-B	✓	✓	X	✓
24109,92-C	✓	✓	✓	✓
24109,92-D	X	X	X	✓
24109,92-E	X	X	X	✓
24210,60-A	✓	✓	✓	X
24210,60-B	✓	✓	X	✓
24210,60-C	✓	✓	✓	✓

bulk of the samples obtained were mare basalts with low TiO_2 and MgO (Ryder et al., 1977). Head et al. (1978) distinguished four different groups of basalt flows in Mare Crisium with the following age relations from oldest to youngest: group I (Fe and Mg rich titaniferous basalts); groups IIB and IIA (regolith derived from very low Ti ferrobasalts, with IIB being less Fe rich); and III (low Ti ferrobasalt). The Luna 24 lander drilled in an area of group IIA basalt. In recent compilations of all ages determined for Luna 24 mare basalts, Burgess and Turner (1998) and Cohen et al. (2001) obtained a unimodal age distribution for these basalts, and concluded that they derived from a single eruptive episode at 3.27 ± 0.08 Ga.

In this paper we present ^{40}Ar-^{39}Ar age determinations of lunar regolith fragments from the Luna 16, 20 and 24 missions. Age studies of these regolith samples are important for constraining the timing of basin formation (Luna 20) and the duration of volcanic event(s) in Mare Fecunditatis (Luna 16) and Mare Crisium (Luna 24). These three sites are situated on the eastern most limb of the near side of the Moon and may therefore have been less influenced by the ejecta originating from within the Procellarum-KREEP Terrain (PKT) as shown by data obtained by Lunar Prospector (Haskin, 1998; Lawrence et al., 1998, 1999; Jolliff et al., 2000; Wieczorek and Phillips, 2000). The Ar data are used to: (1) assess the relative contributions of different Ar components (radiogenic, cosmogenic and solar); (2) determine the crystallisation ages and duration of volcanism within Mare Fecunditatis and Mare Crisium; (3) the timing of impact events; and (4) the cosmic-ray exposure (CRE) age of Luna 16, 20 and 24 fragments.

2. SAMPLES AND EXPERIMENTAL METHODS

The analytical techniques applied to each of the samples are summarised in Table 1. The range of techniques was dependent upon sample size. Where there was sufficient sample, each was subdivided and one portion was examined with a JEOL 6400 scanning electron microscope (SEM) for characterisation of the basaltic texture, and an electron microprobe analyser (EMPA) was used to determine mineral chemical chemistry. The electron microprobe is a five-spectrometer CAMECA SX100 and was used to obtain chemical data from pyroxene, olivine, plagioclase, chromite and ilmenite minerals with on-line data reduction. A cup current of 10 nA with an acceleration potential of 15 keV and an electron beam diameter of ~1 μm was used for individual mineral analyses. For one of the fragments (21013,51-B an impact spherule), bulk analyses were obtained using a defocused beam of 7 μm. The other portion was irradiated and used for age determination using laser probe Ar-Ar dating.

2.1. Sample Descriptions

Samples from Luna 16, 20 and 24 missions were allocated to us by NASA. Samples were from within different layers (depths) of the cores, and each contained a different number of fragments and total weights. Only fragments weighting between 0.2 and 1.3 mg were analysed during this study. Samples were analysed from the following layers of each core: Luna 16 layers 21000 and 21013; Luna 20 layers 220001, 22002 and 22003; and Luna 24 layers 24077, 24109 and 24210 (Table 1). Fragments of sufficient size were split in two pieces: one part for petrographic/chemical study (Figs. 1 and 2) and the other for Ar-Ar analysis. The smallest fragments (≪1 mg) were not subdivided and only used for Ar-Ar analyses. In the next section there are descriptions of those samples that were analysed using SEM and EMPA. The compositions of pyroxenes in Luna 16 and most of the Luna 24 basalts are in agreement with previously reported data (Fig. 2). Sample 24077,92B (brecciated basalt) extends the range of pyroxene composition in Luna 24 basalts to higher Ca levels.

2.1.1. Luna 16

Samples 21000,20-B (0.852 mg), 21000,20-D (0.565 mg), and 21013,51-D (1.155 mg) are fine-grained basalts having ophitic to subophotic textures. The major phases are plagioclase, pyroxene and olivine, with minor ilmenite. The plagioclases of 21000,20-B and 21013,51-D (Fig. 1a) are euhedral to subhedral laths of compositional range $An_{93\text{-}98}$ and $An_{90\text{-}95}$ respectively. Plagioclase laths in 21000,20-D (Fig. 1b) are euhedral to subhedral, occur as blocky to acicular grains (similar to basalt G37 of Steele and Smith, 1972, and 1635 of Snyder et al., 1999) and have a composition of $An_{93\text{-}95}$. Pyroxene and olivine grains are subhedral to anhedral with compositional ranges of $En_{9\text{-}33}Wo_{17\text{-}41}Fs_{29\text{-}63}$ and $Fa_{53\text{-}84}$ respectively. Subhedral olivine grains in sample 21013,51-D are zoned with a core of Fa_{53} and a rim of Fa_{72}. The anhedral olivine grains show a complex texture, possibly caused by an exsolution reaction that was taking place during crystallization. A zoned spinel was analysed and showed the following changes from core to rim: an increase in TiO_2 (from 8.8 to 25.9 wt.%) and FeO (from 36.6 to 54.9 wt.%), and a decrease in Cr_2O_3 (from 32.6 to 12.7 wt.%) and Al_2O_3 (from 17.4 to 3.2 wt.%). Ilmenite grains are acicular, one was zoned showing a decrease in both TiO_2 (from 51.8 to 44.4 wt.%) and FeO (from 43.9 to 43.3 wt.%) from core to rim.

Sample 21013,51-B (1.600 mg) is a green sphere consisting of pyroxene and feldspar micro-lamellae. Bulk chemical analyses of this spherule gave the following data: Al_2O_3 = 18.3 ± 1.0 wt.%, MgO = 13.45 ± 0.48 wt.%, CaO = 11.2 ± 0.2 wt.%, FeO = 10.9 ± 0.2 wt.%, and K_2O = 171 ± 49 ppm. Comparison with previous chemical data for impact melts (summarised in Haskin and Warren, 1991), suggests that this spherule has an impact origin, with the relatively high MgO content being indicative of a basaltic target.

Samples 21000,20-A (1.155 mg) and 21013,51-E (0.439 mg) were inadvertently crushed during splitting or polishing causing loss of their primary textures. Only qualitative mineralogical composition was obtained during SEM examination. EMPA of this sample was not possible due to the convex nature of the surface, which causes interference with beam incidence, a poor ZAF correction and unsatisfactorily low totals. Sample 21000,20-A is a coarse-grained basalt with a crust containing vesicles, and a glassy surface (agglutanitic material), and has zoned phenocrysts (possibly pyroxene and/or olivine). Sample 21013,51-E is also a basalt containing pyroxene, plagioclase, ilmenite and olivine.

Sample 21000,20-C (0.409 mg) was not split and observation was by binocular microscope only. This sample is a basalt with an outer layer containing vesicles and a glassy surface with phenocrysts (possibly pyroxene and/or olivine).

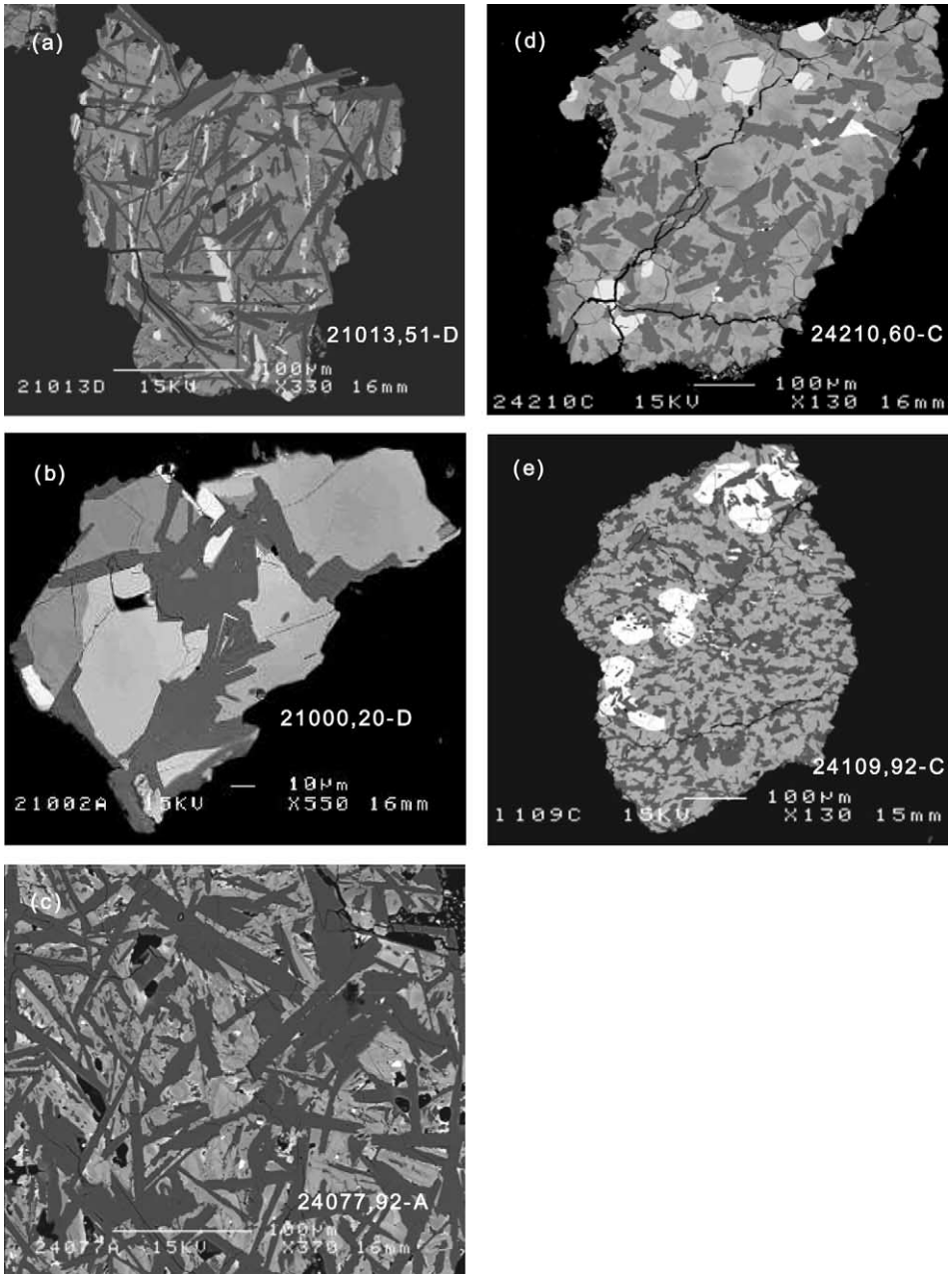

Fig. 1. Backscattered SEM images of representative Luna 16 and 24 basalt fragments. Luna 16: (a) 21013,51-D and (b) 21000,20-D are sub-ophitic basalts comprising mainly laths of plagioclase (dark grey) and subhedral pyroxene (medium grey). Luna 24: (c) 24077,92-A and (d) 24210,60-C are sub-ophitic basalts; (e) 24109,92-C is a metabasalt showing equigranular plagioclase and pyroxene with olivine (white).

2.1.2. Luna 20

Samples analysed were from the upper layers of the regolith core closest to the lunar surface (22001,53, 0.789 mg; 22002,27, 2.768 mg and 22003,34, 6.310 mg) and are composed of regolith fragments < 0.5 mm in diameter. Due to their small size it was not possible to subdivide individual fragments for SEM and Ar-Ar analyses. Instead, approximately half of all the fragments from each layer was characterised using SEM. This revealed that many were basaltic with subophitic to ophitic textures, while others appeared to be metabasalts. Because it was not possible to identify the rock-types of individual fragments, only three of the larger fragments from sample 22003,34 were selected for Ar-Ar analyses.

2.1.3. Luna 24

Samples 24077,92-A (2.152 mg) and 24210,60-C (0.679 mg) are fine-grained basalts with sub-ophitic textures (Figs. 1c and 1d). Sample 24077,92-A (Fig. 1c) shows two areas of different grain size separated by a well-defined plagioclase border. The major phases present in both samples are plagioclase, pyroxene and olivine. The plagioclases are euhedral to subhedral, acicular laths with a composition of $An_{95\text{-}99}$. The pyroxene grains are anhedral with a composition $En_{15\text{-}40}Wo_{7\text{-}35}Fs_{37\text{-}70}$ (Fig. 2). Olivine grains in sample 24077,92-A are small and scarce and have composition Fa_{63}. In 24210,60-C olivine occurs as phenocrysts with compositions in the range $Fa_{88\text{-}89}$. The composition of plagioclase,

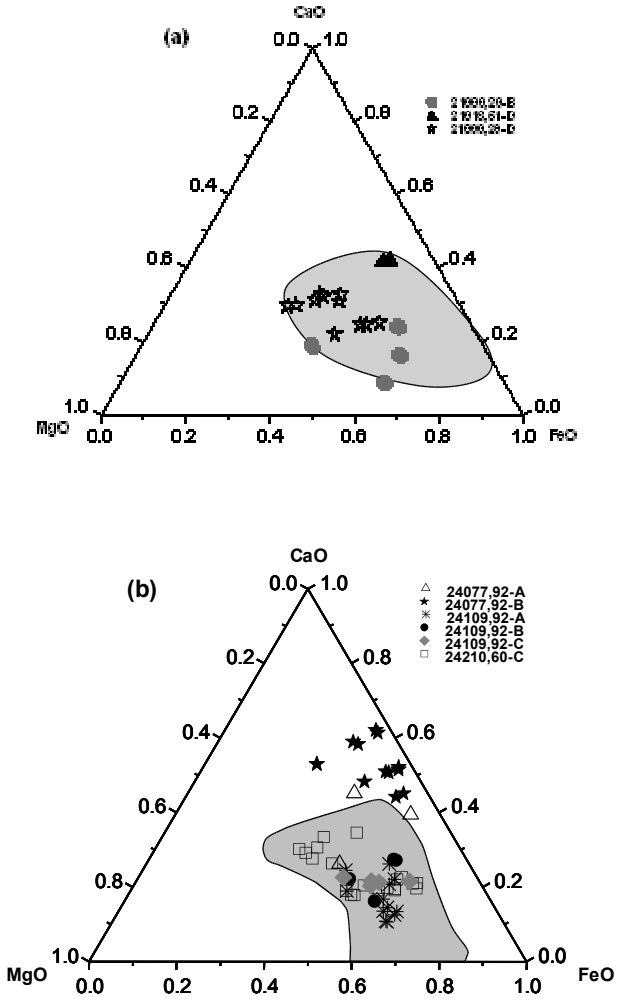

Fig. 2. CaO-MgO-FeO composition of pyroxene in (a) Luna 16 basalts and (b) Luna 24 basalts. Shaded area corresponds to pyroxene data from the literature for Luna 16 (Albee et al., 1972; Grieve et al., 1972; Hollister and Kulick, 1972; Steele and Smith, 1972) and Luna 24 (Ryder et al., 1977; Vaniman and Papike, 1977; Coish and Taylor, 1978; Taylor et al., 1991; Papike et al., 1998; Papike and Vaniman, 1978).

pyroxene (Fig. 2) and olivines are similar to those reported previously by Ryder et al. (1977) for Luna 24 very low titanium (VLT) basalts.

Sample 24077,92-B (1.050 mg) is a highly fractured brecciated basalt. The pyroxenes compositions are augite ($En_{43-53}Wo_{11-23}Fs_{30-44}$) and low-Ca ($En_{38-56}Wo_{3-8}Fs_{38-55}$) and are outside the range defined by Luna 24 basalts being more Ca-rich (Fig. 2).

Samples 24109,92-A (0.911 mg) and 24109,92-B (0.560 mg) are coarse-grained basalts consisting of euhedral to subhedral plagioclase and pyroxene with minor olivine. The plagioclase composition in all three samples is An_{96-99}. The pyroxenes compositions are: 24109,92-A is $En_{9-22}Wo_{18-26}Fs_{53-67}$; and 24109,92-B is $En_{14-23}Wo_{16-29}Fs_{52-61}$. In 24109,92-A the olivine grains have a chemical composition of Fa_{91}. The composition of olivines in 24109,91-B is Fa_{88}.

Sample 24109,92-C (0.555 mg) is a fine-grained metabasalt containing equigranular plagioclase and pyroxene with olivine phenocrysts (Fig. 1e) in the range Fa_{87-88}. Previously, it has been shown that the Luna 24 metabasalts are isochemical with the ophitic basalts (Laul et al., 1978) and are believed to have been formed by contact metamorphism with overlying lava flows (Ryder et al., 1977).

Samples 24210,60-A (4.084 mg) and 24210,60-B (0.683 mg) are regolith breccias. Sample 24210,60-A contains abundant feldspar and pyroxene fragments and lesser olivine fragments. The chemical composition of the plagioclases is An_{91-99} and that of the pyroxene is $En_{13-32}Wo_{15-28}Fs_{41-70}$. Sample 24210,60-B contains large feldspathic clasts within a matrix composed mainly of small clasts of feldspar and pyroxene. No EMPA analyses were performed.

The following samples were too small to be subdivided for separate SEM characterisation: 24077,92-C (0.257 mg); 24077,92-D (0.396 mg); 24077,92-E (0.271 mg); 24109,92-D (0.343 mg) and 24109,92-E (0.201 mg). The description of these samples is based on binocular-microscope observation only. They appeared to be basalts with an outer glassy layer containing vesicles. Samples 24077,92-D, 24077,92-E and 24109,92-D showed the existence of greenish phenocrysts (possibly pyroxene and/or olivine).

2.2. Irradiation, Laser Stepped Heating, and Data Reduction Procedures

Prior to Ar-Ar analyses, the samples were positioned between Hb3gr monitors and vacuum sealed in silica vials and then irradiated. Fragments of Luna 16 and 20 were irradiated at the Risø reactor in Denmark with a fast neutron fluence of 3.6×10^{18} neutrons cm^{-2} (irradiation MN14). Luna 24 samples were irradiated at the Sacavém reactor in Portugal with a fast neutron fluence of 2.4×10^{18} neutrons cm^{-2} (irradiation MN16). Within each vial, normally five samples were positioned between two monitors over a total distance of ≤ 2 cm. The difference in J value between the two monitors within the same vial is $\sim$1%, which is $\sim$3 times higher than the uncertainty on an individual J value. Therefore, a 1% uncertainty has been used in calculating individual step ages (given in the Electronic Annex), and 1.4% uncertainty on J, introduced from the error on the age determination of the Hb3gr monitor (1072 $\pm$ 11 Ma; Turner et al., 1971; Roddick, 1983), is included for calculation of the total and plateau ages.

The Ar-Ar extraction technique used was infra-red (IR) laser stepped heating using a defocused Nd-YAG (λ = 1064 nm) laser beam of $\sim$3 mm diameter. Methods are described in detail by Burgess and Turner (1998) and Fernandes et al. (2000), and briefly consisted of heating each fragment over 10 to 52 steps of increasing laser output power (corresponding to an increase in temperature). Each heating step was of 1-min duration, followed by another 9-min gas clean-up using a Zr-Al getter at 250°C. Raw data were corrected for background, mass discrimination, radioactive decay of ^{37}Ar, and neutron interference reactions on Ca, K and Cl. All errors are given at one standard deviation level. Combined blank and background levels of Ar were measured by 10-min isolation of the laser port from the pumps without laser heating. Blanks were run at the start of each day and after every third heating step. Average blank levels and their variability (1 standard deviation) over the course of these experiments, in units of 10^{-14} cm^3 STP, are equivalent to the following: (1) Luna 16, $^{40}Ar = 882 \pm 68$; $^{39}Ar = 27 \pm 2$; $^{38}Ar = 53 \pm 2$; $^{37}Ar = 32 \pm 1$; $^{36}Ar = 90 \pm 10$; (2) Luna 20, $^{40}Ar = 864 \pm 7$; $^{39}Ar = 27 \pm 2$; $^{38}Ar = 32 \pm 2$; $^{37}Ar = 32 \pm 2$; $^{36}Ar = 82 \pm 2$; and for (3) Luna 24, $^{40}Ar = 504 \pm 59$; $^{39}Ar = 3.8 \pm 0.4$; $^{38}Ar = 4.8 \pm 0.4$; $^{37}Ar = 5.9 \pm 0.2$; $^{36}Ar = 14 \pm 1$.

2.3. Argon Mixing Diagram for the Lunar Regolith and Method of Age Calculation

Lunar regolith samples can potentially contain argon from several different sources including solar wind, cosmogenic and radiogenic components. The use of stepped heating can enable partial or complete resolution of these components because solar argon is primarily trapped on the surfaces of grains and will therefore be released at relatively low temperatures compared to radiogenic and cosmogenic Ar, which will be uniformly distributed throughout the grain volume. The volume-related components will dominate the Ar release at higher temperature. The measured ^{36}Ar values are corrected for cosmogenic ^{36}Ar ($^{36}Ar_t$) by assuming cosmogenic $^{36}Ar/^{38}Ar = 0.65$ for this component, however the effect of this correction is usually small. The corrected data can be represented on a three isotope diagram of $^{36}Ar_t/^{40}Ar$ vs. $K/^{40}Ar$ (or $^{40}Ar/^{36}Ar_t$ vs. $K/^{36}Ar_t$) as a mixture of solar Ar, trapped Ar (including re-trapped lunar atmospheric ^{40}Ar) and ^{40}Ar (from *in situ* radioactive decay of ^{40}K) and K-derived ^{39}Ar (from the nuclear irradiation). In the present study, the measured ^{39}Ar has been converted to K, the plot most used is $^{36}Ar_t/^{40}Ar$ vs. $K/^{40}Ar$ (Fig. 3). Because solar Ar is released from the surface of grains at relatively low temperature, the medium to high

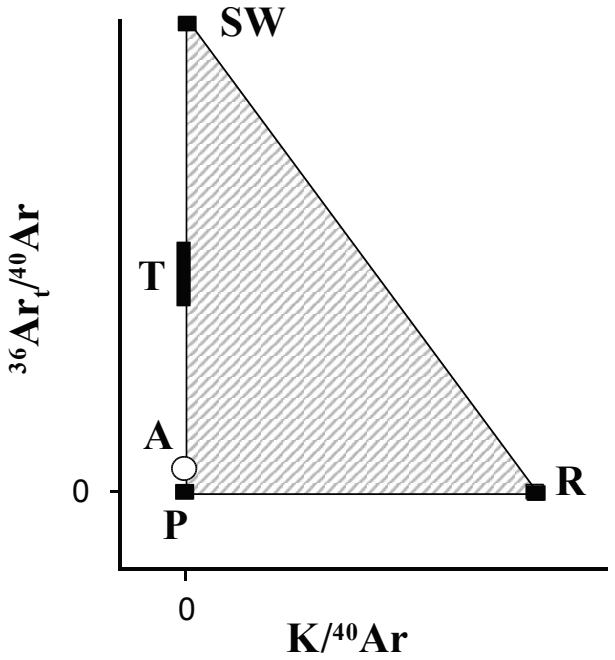

Fig. 3. Argon isotope correlation diagram showing the relative position of different argon components: trapped (T) argon in lunar soil grains is usually interpreted to be a mixture of parentless (P) argon, implanted from the lunar atmosphere and solar wind (SW) argon, the trapped component is usually sited at the edges of soil grains. The radiogenic component is formed by in situ decay of ^{40}K and is present throughout the whole volume of the grains. During stepped heating the composition changes from P → T → R and a linear correlation between T and R can be extrapolated to obtain the crystallisation age. In effect, points can lie anywhere in the shaded triangle but rarely exceed trapped ratios of $^{36}Ar_t/^{40}Ar$ between 1 and 2. Lunar samples have been exposed to the terrestrial atmosphere (A) so this component can also be present as a contaminant adsorbed onto sample surfaces and will be released at low temperature during stepped heating.

temperature release forms a linear correlation interpreted as a binary mixture of trapped Ar with a $^{36}Ar/^{40}Ar$ value given by extrapolation to $^{39}Ar/^{40}Ar = 0$, and radiogenic ^{40}Ar with $^{40}Ar/^{39}Ar$ given by extrapolation to $^{36}Ar_t/^{40}Ar = 0$. The relationships between the different Ar components are shown in Fig. 3. Some samples do not yield linear correlations on the mixing diagram. This may be due to the sample being a mixture of mineral or lithic clasts that have suffered different degrees of exposure at the lunar surface, or where trapped ^{40}Ar is the overwhelmingly dominant component in the sample. In these cases, the minimum measured $^{40}Ar/^{36}Ar_t$ value is assumed to approximate the trapped ratio and is used to correct the measured $^{40}Ar/K$ of each heating step. Usually a correction involving the minimum $^{40}Ar/^{36}Ar_t$ value should lead to a slight over-correction for trapped Ar and thus a minimum age of the sample would be obtained. In either case of using the maximum or extrapolated ratios, apparent ages which have been corrected for trapped argon should converge at high temperature, with those which have not been corrected, because release from interior regions of samples are less influenced by trapped argon.

Where appropriate, Ar-Ar ages are calculated from $^{36}Ar_t/^{40}Ar$ vs. $K/^{40}Ar$ plots that show good linear correlations. Intercept $K/^{40}Ar$ values and errors are obtained from least squares fitting using the method of Williamson (1968). These fits also yield trapped $^{36}Ar_t/^{40}Ar$ compositions which are used to correct apparent ages which are shown in the form of age spectra, and the error on the trapped Ar ratio has been propagated through the age equation. Event ages calculated from age spectrum diagrams, or where linear correlations are not present, are from sections of the age spectrum with reasonably consistent step ages amounting to > 50% of the Ar release. An average event age and error are calculated by weighting each step according to the fraction of ^{39}Ar release. It is noted that in most cases these are not intended to be plateau ages but usually they represent the interval of ^{39}Ar release over which apparent ages converge following correction for trapped Ar. Combined ages calculated from steps comprising < 50% ^{39}Ar release are also weighted averages but in these cases, the age range is taken to be a more appropriate reflection of the variation.

3. RESULTS

3.1. Luna 16

Apparent age spectra, K/Ca and isotope correlation diagrams for five Luna 16 basalts and one impact glass are shown in Fig. 4, and the data are summarised in Table 2. The age spectra are shown for apparent ages that have not been corrected for trapped Ar ($^{40}Ar/^{36}Ar_t = 0$, solid spectrum) and those which have, based on either an isotope correlation diagram or the minimum measured $^{40}Ar/^{36}Ar_t$ values ($^{40}Ar/^{36}Ar_t > 0$, open spectrum) as discussed previously. Data are corrected for cosmogenic ^{36}Ar assuming $^{38}Ar/^{36}Ar = 1.54$, and trapped argon using the $^{40}Ar/^{36}Ar_t$ ratio for each sample given in Table 1. Isotope correlation plots (Figs. 4–6) shown uncorrected data (open symbols) and after correction for spallation production of ^{36}Ar (solid symbols). Ages reported are for data corrected for $^{40}Ar/^{36}Ar_t$ unless otherwise indicated. The amounts and isotopic composition of the Ar released by stepped heating are given in the Electronic Annex.

The age spectra for basalts 21000,20-A, 21000,20-B, 21000,20-D (Fig. 4a) are complex and the interpretation is not straightforward. These samples contain relatively high concentrations of trapped Ar making correction procedures very sensitive to the choice of $^{40}Ar/^{36}Ar$ value used for this component, thus caution in the interpretation of the data must be exercised. Since the data from none of these samples form linear correlations on a $^{36}Ar_t/^{40}Ar$ vs. $K/^{40}Ar$ diagram (Fig. 4a), the correction for trapped argon was attempted using the lowest measured values for $^{40}Ar/^{36}Ar_t$ of between 0.84 and 0.90 (Table 2). This approach will almost certainly over-estimate the level of trapped ^{40}Ar in the samples meaning that the apparent ages of ≤ 3.3 Ga (21000,20-A), ≤ 3.4 Ga (21000,20-B) and ≤ 4.03 Ga (21000,20-D) should be considered as lower limits of their actual ages (Table 2).

The age spectrum for 21013,51-B impact spherule (Fig. 4b) shows the presence of trapped Ar components with anomalously old apparent ages dominating over 70% of the ^{39}Ar release. Correction for trapped ^{40}Ar for these steps, based on the minimum measured $^{40}Ar/^{36}Ar_t$ value of 0.94, does not adequately account for the trapped Ar (Fig. 4b). However, the last 28% of ^{39}Ar release does not contain appreciable trapped ^{40}Ar and gives young apparent ages of 0.933 to 1.078 Ga with a total age of 0.988 ± 0.010 Ga. This age is most likely indicative of an impact event in the vicinity of the Luna 16 landing site.

Basalt 21013,51-D showed negligible amounts of trapped Ar (Fig. 4c), and the total age, calculated by summing argon released over all the temperature steps, is 3.32 ± 0.02 Ga. Excluding the initial 19% of ^{39}Ar release, which shows evidence for ^{40}Ar loss, the remaining 81% of the ^{39}Ar gives an age of 3.37 ± 0.02 Ga. Over this region of the age spectrum the K/Ca value decreases from 0.02 to 0.01 probably representing argon released from both pyroxene and plagioclase, which have

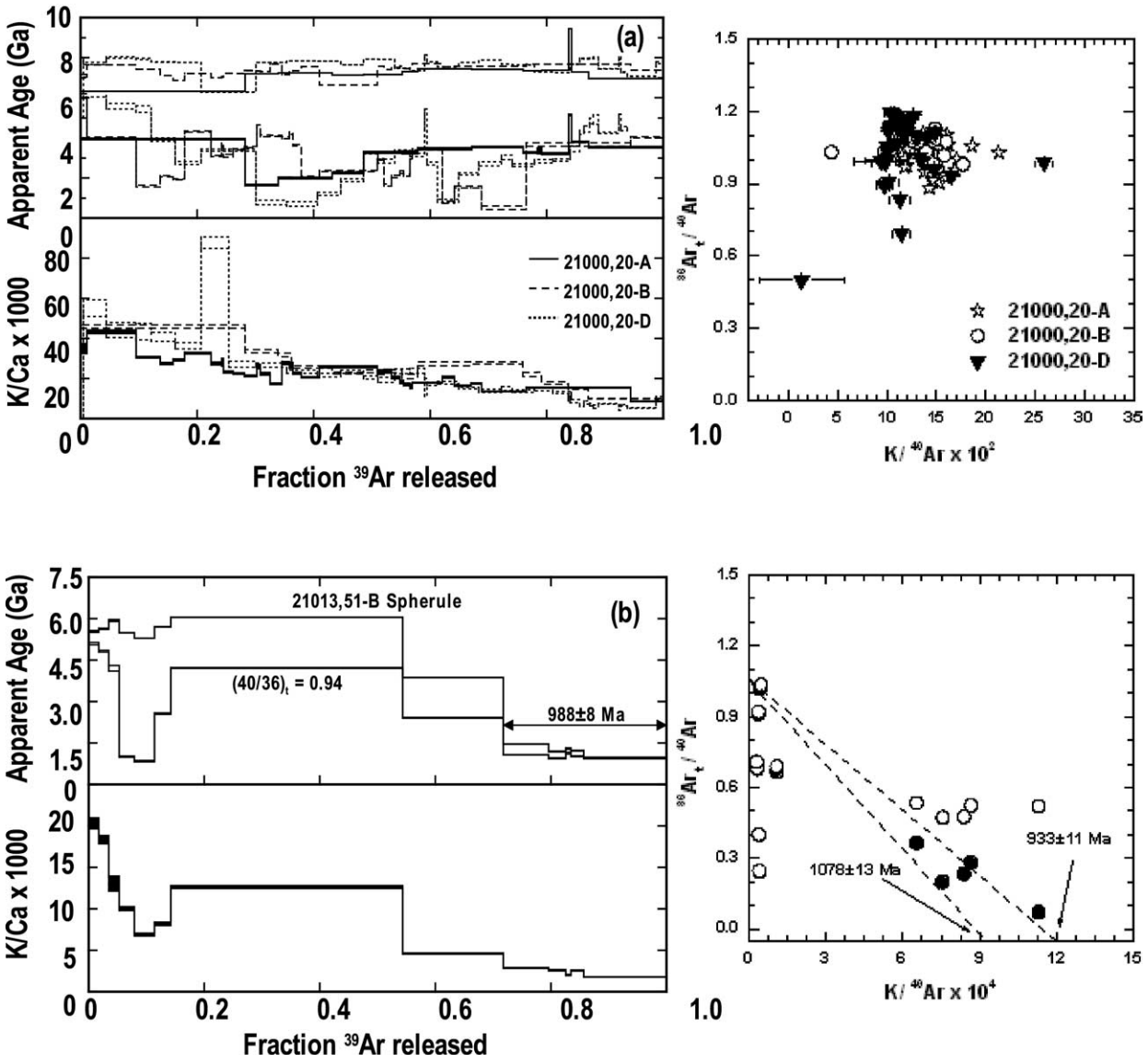

Fig. 4. Age spectrum, K/Ca vs. ^{39}Ar release and isotope correlation diagrams for Luna 16 samples (Turner and Cadogen, 1974): (a) 21000,20-A, 21000,20-B and 21000,20-D; (b) 21013,51-B; (c) 21013,51-D; and (d) 21013,51-E. In (b) to (d) solid age spectrum diagrams represent apparent ages that are uncorrected for trapped ^{40}Ar components (^{40}Ar/^{36}Ar$_t$ = 0), but are corrected for cosmogenic components. The open age spectra have been corrected using the trapped ^{40}Ar/^{36}Ar values shown on the figure. For the plots on the right, solid symbols in (a) to (d) show the minor effects of correcting for cosmogenic ^{36}Ar.

K/Ca of 0.033 to 0.0129 and 0.0015 to 0.0067 respectively as determined by EMPA.

Sample 21013,51-E (Fig. 4d) shows a flat age spectrum over 96% of ^{39}Ar release with apparent ages $>$ 4.5 Ga. It is only during the final 4% of ^{39}Ar release that the apparent ages decrease to $<$ 4.5 Ga. On a plot of ^{36}Ar$_t$/^{40}Ar vs. K/^{40}Ar (Fig. 4d) data show a poorly defined correlation between trapped ^{36}Ar$_t$/^{40}Ar and radiogenic ^{40}Ar components, however, extrapolation to the K/^{40}Ar axis gives an age of 3.36 $\pm$ 0.34 Ga. Correction of the data for trapped ^{40}Ar are based on the minimum measured ^{40}Ar/^{36}Ar$_t$ value of 1.04 (a value commonly observed for lunar samples) gives a similar age of 3.35 $\pm$ 0.04 Ga (Fig. 4d). This age is within the range reported previously for basalts from Mare Fecunditatis (Huneke et al., 1972; Cadogan and Turner, 1977; Cohen et al., 2001).

Due to a mistake in the laser power output setting, only one shot was acquired at very high power for sample 21000,20-C; the apparent age is high $>$ 4.5 Ga and does not allow any constraint on the ^{40}Ar/^{36}Ar of trapped argon. Correcting for trapped Ar is highly dependent upon the ^{40}Ar/^{36}Ar value that is used, e.g. a wide variation in potentially realistic ages of 2.0 to 4.5 Ga are obtained within a relatively narrow range of ^{40}Ar/^{36}Ar values between 1.30 and 1.45. Thus, we are unable to obtain a meaningful age interpretation for 21000,20-C.

In summary, the apparent ages of two Luna 16 basalts of 3.37 Ga (21013,51-D) and 3.35 Ga (21013,51-E) are inter-

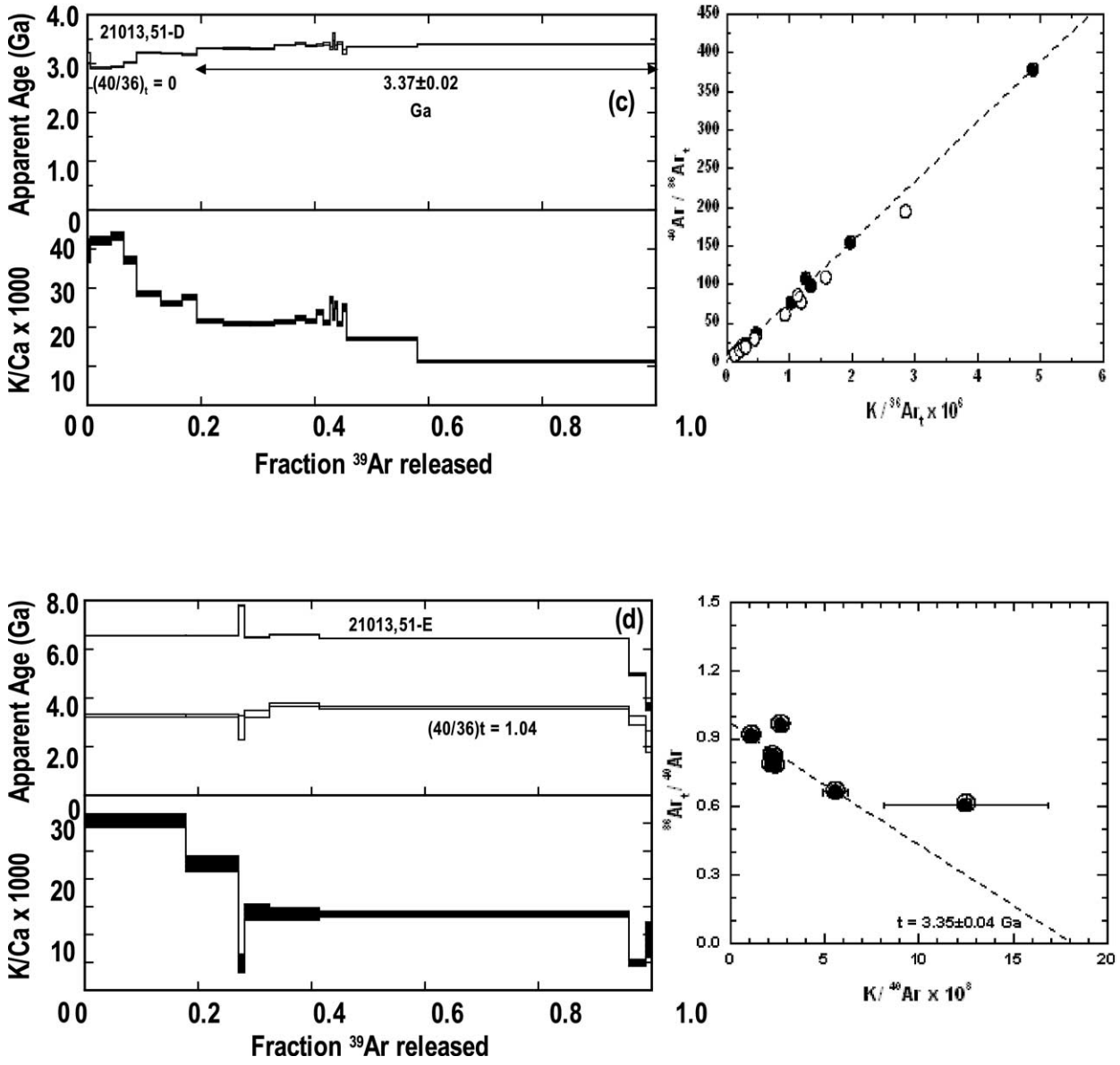

Fig. 4. (Continued)

preted to be crystallisation ages representing a single period of volcanic activity (Table 2). Three samples from layer 21000,20 are contaminated with relatively high levels of trapped Ar giving high apparent ages that are difficult to interpret, however an attempt to correct for the presence of trapped Ar resulted in minimum apparent ages of 3.3 Ga. The young apparent age

Table 2. Summary of Ar-Ar ages of Luna 16 regolith fragments obtained by IR-laser stepped heating.

Sample	Lithology	K (ppm)[a]	Ca (wt.%)[a]	K/Ca[b] ($\times 10^3$)	Age (Ga)	CRE-age (Ma)	$(^{40}Ar/^{36}Ar)_t$
21000,20-A	Basalt	298	1.57	19.4	≤3.29 ± 0.05	nd[c]	0.90 ± 0.0007
21000,20-B	Fine-grain basalt	319	1.43	20	≤3.38 ± 0.03	nd[c]	0.89 ± 0.0007
21000,20-D	Fine-grain basalt	106	0.67	20	≤4.03 ± 0.03	nd[c]	0.84 ± 0.001
21013,51-B Spherule	Impact glass	106	2.35	5	0.988 ± 0.008[b]	470	0.94 ± 0.0008
21013,51-D	Fine-grain basalt	376	2.43	14	3.37 ± 0.02	151	0
21013,51-E	Coarse-grain basalt	15	0.10	0.53	3.35 ± 0.04	1280	1.04 ± 0.01

[a] K and Ca reported were calculated based on the ^{39}Ar and ^{37}Ar released during laser heating.
[b] Lowest apparent age in the age spectrum possibly related to an impact event.
[c] Not determined due to $^{38}Ar/^{36}Ar$ being mostly trapped.

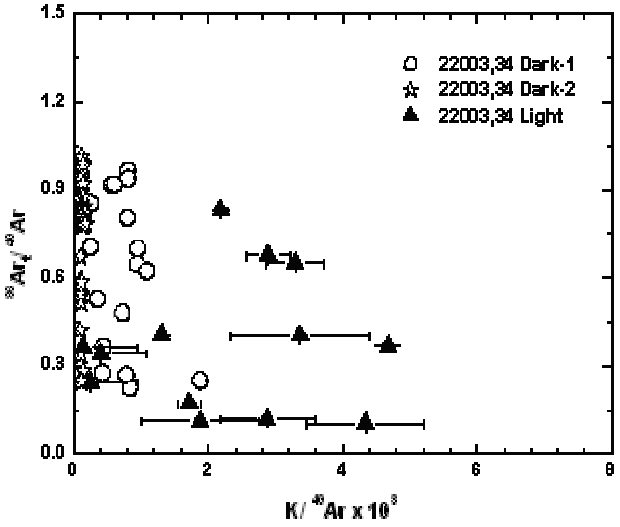

Fig. 5. $^{40}Ar/^{36}Ar$ vs. $K/^{36}Ar$ correlation diagram for three different fragments of Lunar 20 sample 22003,34.

obtained from 21013,51-B impact spherule of 0.988 Ga is considered to record the timing of an impact event in the vicinity of the Luna 16 site.

3.2. Luna 20

Two dark and one light-coloured fragments were separated from the fine regolith fraction ($\ll$1 mm diameter) of 22003,34 for Ar-Ar analyses. The amounts and isotopic composition of the Ar released by laser stepped heating are given in the Electronic Annex. The three fragments show a high content of trapped ^{40}Ar, and it is not possible to distinguish trapped from *in situ* radiogenic ^{40}Ar using a $^{36}Ar_t/^{40}Ar$ vs. $K/^{40}Ar$ diagram (Fig. 5). Even using the highest measured $^{36}Ar_t/^{40}Ar$ value for each sample to correct for trapped Ar, the apparent ages are not reduced to $<$ 4.5 Ga, indicating the overwhelming dominance of trapped ^{40}Ar (>75% of the total ^{40}Ar) within these fragments. Since most of the ^{40}Ar present in these samples is not a product of radioactive decay, it is not possible to obtain meaningful ages.

3.3. Luna 24

Apparent age spectra, K/Ca and isotope correlation diagrams for nine Luna 24 basalts and one breccia are shown in Fig. 6, the data are summarised in Table 3. The amounts and isotopic composition of the Ar released by laser stepped heating are given in the Electronic Annex.

The first six heating steps of 24077,92-A (fine-grained basalt) show a steady increase in the $^{36}Ar_t/^{40}Ar$ until a maximum value of 1.12 is reached (Fig. 6a). The Ar released over these initial steps is interpreted to be a mixture of parentless ^{40}Ar and solar wind ^{36}Ar residing close to the grain boundaries; all these steps give anomalously high apparent ages. The intermediate and high temperature steps, corresponding to 71% of the total ^{39}Ar released, show a steady decrease in $^{36}Ar_t/^{40}Ar$ coupled with increasing $K/^{40}Ar$ values and data form a linear correlation on a $^{36}Ar_t/^{40}Ar$ vs. $K/^{40}Ar$ diagram. This correlation is interpreted as a binary mixture of trapped Ar with $^{40}Ar/^{36}Ar_t$ of 1.19 (intercept on $^{36}Ar_t/^{40}Ar$ axis) and radiogenic ^{40}Ar with $K/^{40}Ar$ corresponding to an age of 2.52 $\pm$ 0.03 Ga. Following correction for trapped Ar, these steps form a plateau on the age spectrum (Fig. 6a, open spectrum), which converges with the uncorrected data at high temperature. The low K/Ca of $\sim$0.0034 for the flat region of the ^{39}Ar release spectrum, is assumed to represent Ar release from plagioclase.

Data obtained during Ar-Ar analysis of the basalt samples 24077,92-B and 24077,92-D do not show well-defined correlations on a $^{36}Ar_t/^{40}Ar$ vs. $K/^{40}Ar$ diagrams (Figs. 6b and 6c). The $^{40}Ar/^{36}Ar_t$ value of the trapped argon component is estimated to be the minimum value measured during stepped heating of 0.78 and 0.50 for 24077,92-B and 24077,92-D respectively. For 24077,92-B, correction of the measured ^{40}Ar content for trapped Ar leads to a combined age of 3.96 $\pm$ 0.08 Ga for the high temperature steps comprising 62% of the total ^{39}Ar release. The K/Ca ratios corresponding to this release are in the range of 0.0010 to 0.0036 (Fig. 6b). This is indistinguishable from the EMPA analysis of plagioclase yielding a K/Ca ratio of 0.0013. Sample 24077,92-D shows evidence for possible disturbance at $\sim$0.53 Ga (intermediate temperature steps in Fig. 6c). During the last 22% the ^{39}Ar release, which is largely devoid of trapped Ar, an apparent age of 3.42 $\pm$ 0.18 Ga is obtained.

A similar approach has been used to interpret data for basalt samples 24077,92-E (Fig. 6d), 24109,92-A (Fig. 6e), 24109,92-C (Fig. 6f), 24210,60-C (Fig. 6h; for ease of discussion this sample is considered here before 24109,92-B in Fig. 6g) where Ar data show binary mixing on plots of $^{36}Ar_t/^{40}Ar$ vs. $K/^{40}Ar$. The trapped $^{40}Ar/^{36}Ar_t$ values are between 0.41 (24109,92-C) and 0.51 (24077,92-E) with apparent ages of 24077,92-E = 3.20 $\pm$ 0.06 Ga, 24109,92-A = 3.09 $\pm$ 0.13, 24109,92-C $\pm$ 3.16 $\pm$ 0.13 and 24210,60-C = 3.45 $\pm$ 0.09 (Table 3). 24210,60-C differs in that 30% of the ^{39}Ar released at high temperature gives a low apparent age of 1.70 $\pm$ 0.01 Ga. The cause of this low age is unclear; it is possible that the sample has been affected by recoil of ^{39}Ar (Turner and Cadogen, 1974), although it is not evident in any other samples, or it could be partial re-setting of the K-Ar system during a later impact event. In comparison with other Luna 24 samples analysed in this study, the K/Ca values of 24077,92-E (Fig. 6d), 24109,92-A (Fig. 6e), 24109,92-C (Fig. 6f) and 24210,60-C (Fig. 6h) are lower, within the range 0.001 to 0.006. This is similar to the K/Ca range determined for plagioclase by EMPA in 24109,92-C and 24210,60-C of 0.001 to 0.004.

Sample 24109,92-B (coarse-grained basalt) contains a small amount of trapped argon with a minimum $^{40}Ar/^{36}Ar_t$ = 0.31 (Fig. 6g). With the exception of the low temperature heating steps, most data are clustered close to the $K/^{40}Ar$ axis on a plot of $^{36}Ar_t/^{40}Ar$ vs. $K/^{40}Ar$ (Fig. 6g). The first 1% ^{39}Ar release gives a high apparent age, $>$ 4.5 Ga, followed by a decrease in apparent age to $\leq$ 0.6 Ga for the following 5% of ^{39}Ar release. For the remaining 94% ^{39}Ar release, apparent ages are relatively constant for each heating step giving a combined age of 3.37 $\pm$ 0.04 Ga (Fig. 6g). Over this interval of ^{39}Ar release, the K/Ca value is relatively constant at $\sim$0.0025. This K/Ca value is within the range of that obtained during EMPA of plagioclase in this sample of between 0.00082 and 0.00268.

Basalt 24109,92-E contains a relatively large amount of

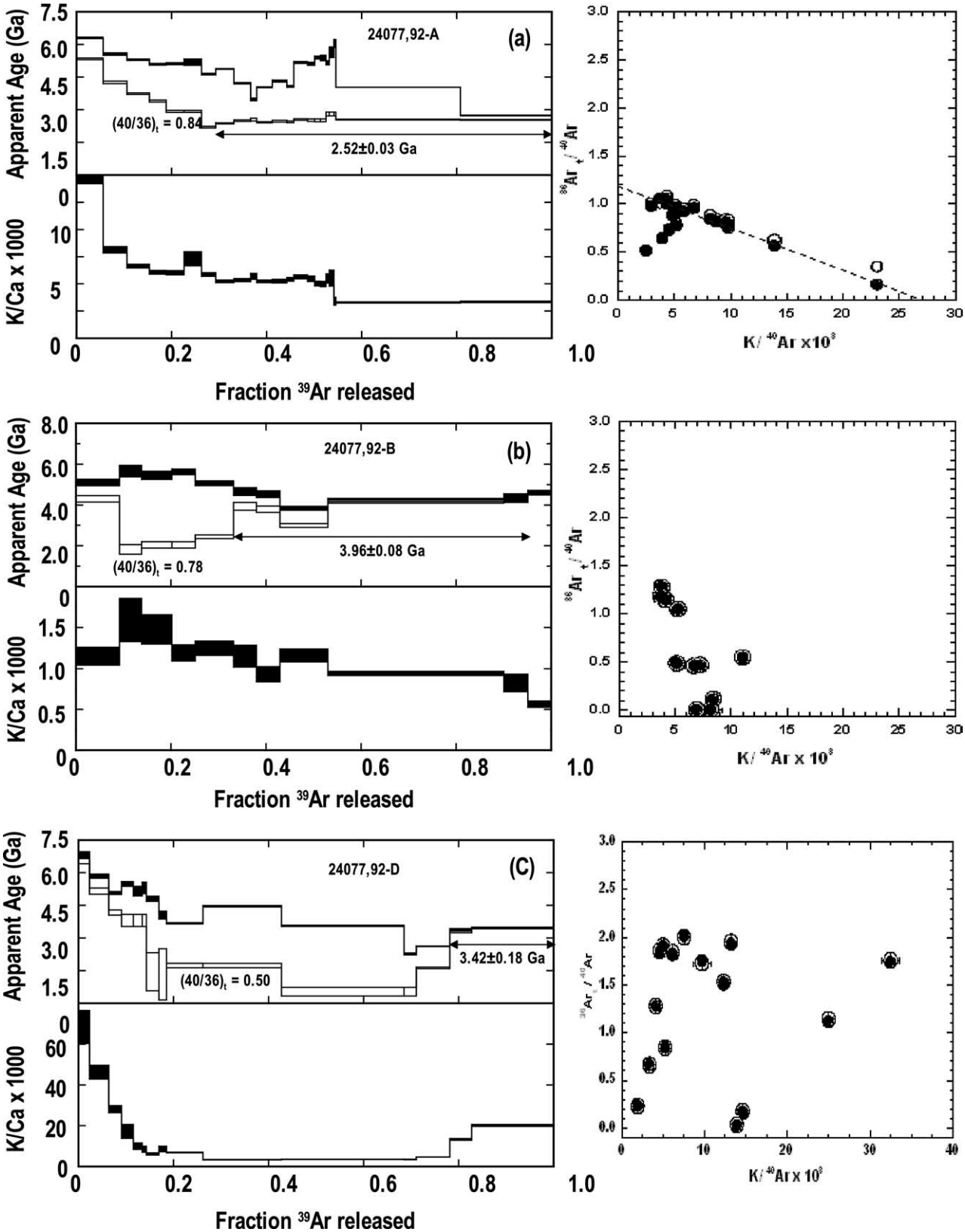

Fig. 6. Age spectrum, K/Ca vs. ^{39}Ar release and isotope correlation diagrams for Luna 24 basalts: (a) 24109,92-B; (b) 24077,92-B; (c) 24077,92-A;(d) 24109,92-A; (e) 24109,92-C; (f) 24210,60-C;(g) 24077,92-E; (h) 24077,92-D; (i) 24210,60-B. See Figure 4 for explanation of symbols.

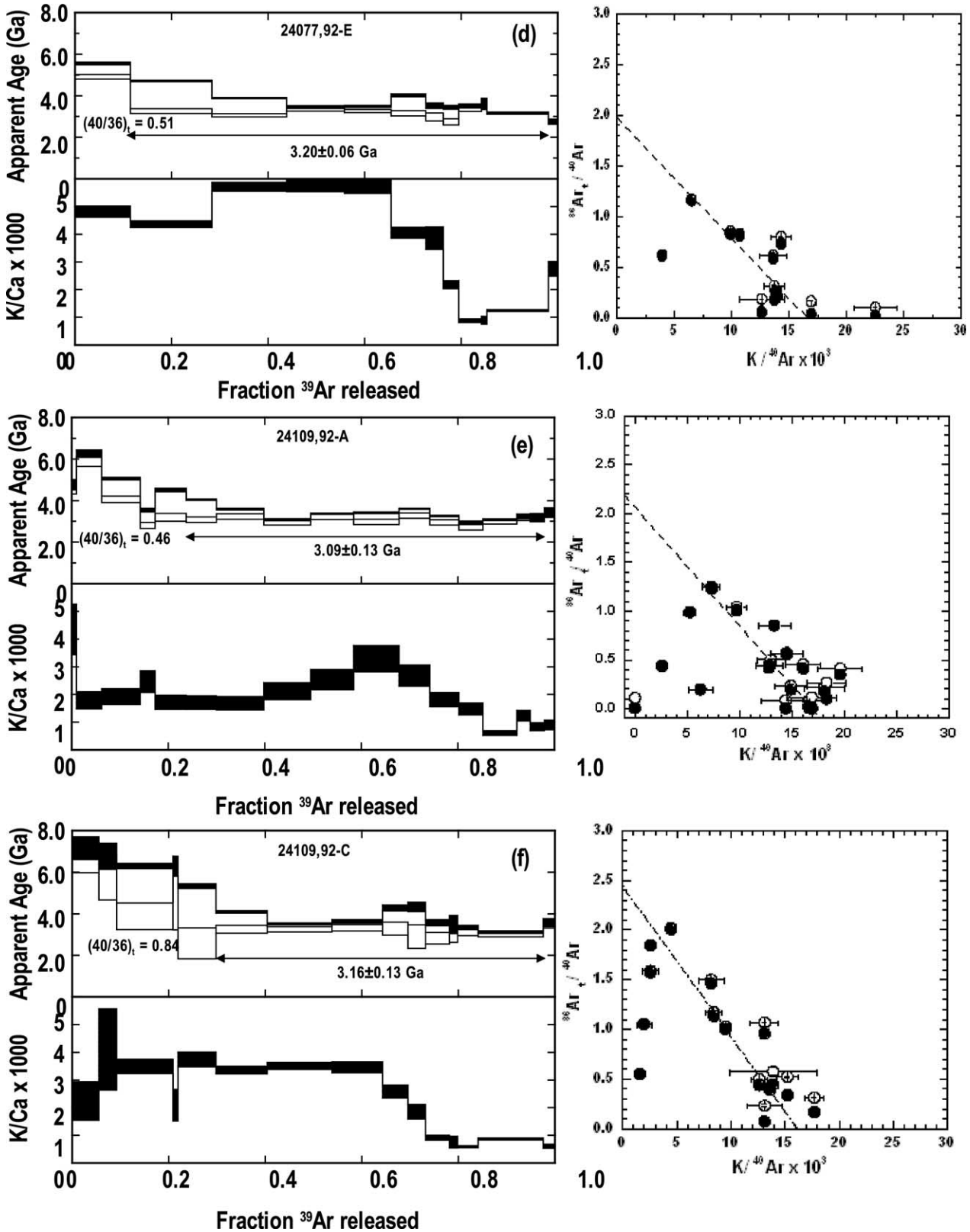

Fig. 6. (Continued)

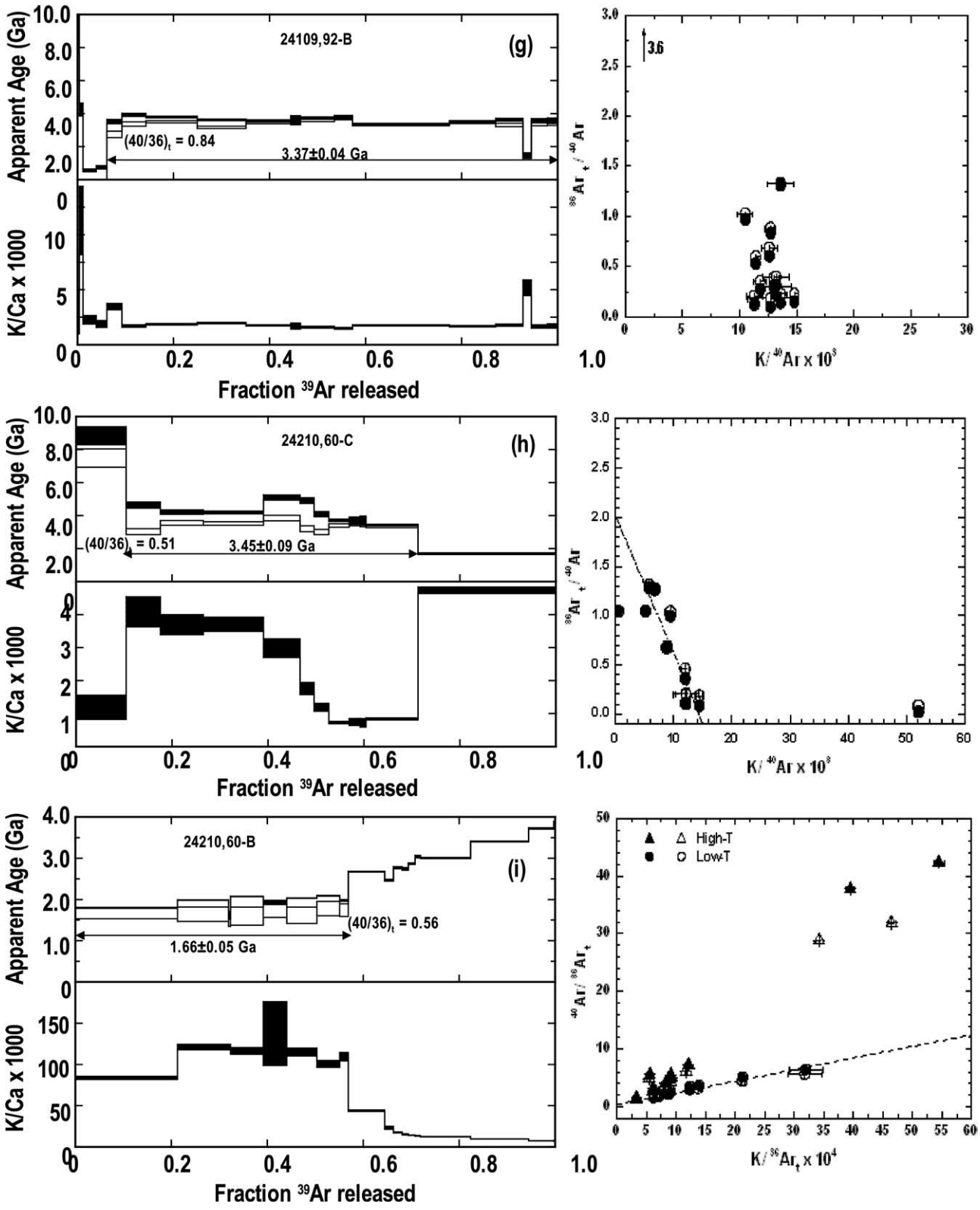

Fig. 6. (Continued)

Table 3. Summary of Ar-Ar data of Luna 24 regolith fragments obtained by IR-laser stepped heating.

Sample	Lithology	K (ppm)[a]	Ca (wt.%)[a]	K/Ca ($\times 10^3$)	Age (Ga)	CRE-age (Ma)	$(^{40}Ar/^{36}Ar)_t$
24077,92-A	Fine-grain basalt	54.05	1.23	5.0	2.52 ± 0.03	1642 ± 69	0.84 ± 0.01
24077,92-B	Brecciated basalt	12.80	1.26	1.0	3.96 ± 0.08	35 ± 1	0.78 ± 0.01
24077,92-D	Basalt	59.79	1.09	5.5	3.42 ± 0.18	147 ± 3	0.50 ± 0.01
24077,92-E	Basalt	59.68	2.09	2.9	3.20 ± 0.06	519 ± 8	0.51 ± 0.01
24109,92-A	Coarse-grain basalt	65.26	4.13	1.6	3.09 ± 0.13	284 ± 4	0.46 ± 0.04
24109,92-B	Coarse-grain basalt	59.49	3.51	1.7	3.37 ± 0.04	443 ± 6	0.31 ± 0.01
24109,92-C	Fine-grain basalt	21.49	1.18	1.8	3.16 ± 0.13	518 ± 7	0.41 ± 0.03
					3.72 ± 0.01[c]		0
24210,60-B	Breccia	287.14	1.16	24.9	1.66 ± 0.05[b]	211 ± 3	0.56 ± 0.05
24210,60-C	Coarse-grain basalt	22	1.15	1.9	3.45 ± 0.09	343 ± 4	0.51 ± 0.02

[a] K and Ca reported were calculated based on the ^{39}Ar and ^{37}Ar released during laser heating
[b] Lowest apparent age in the age spectrum possibly related to an impact event.
[c] Maximum temperature step age.

trapped argon and there is no correlation on a plot of $^{36}Ar_t/^{40}Ar$ vs. $K/^{40}Ar$ diagram (not shown). Apparent ages calculated using the lowest $^{40}Ar/^{36}Ar_t$ value of 0.55, show a progressive decrease with temperature to a minimum value of 1.11 Ga over the final 15% of ^{39}Ar release. Samples 24109,92-D and 24077,92-C also contain high levels of trapped argon, and still give ages of $>$ 4.5 Ga after correction for trapped argon using the lowest measured $^{40}Ar/^{36}Ar_t$ for each sample.

The apparent age spectrum for breccia 24210,60-B is complex and distinct from that of the basalt samples and this sample appears to record more than one age event as indicated by data showing two trends on a plot of the $^{40}Ar/^{36}Ar_t$ vs. $K/^{36}Ar$ (Fig. 6i). This is reflected in the age spectrum plot as a sharp change in apparent ages and K/Ca values after 57% ^{39}Ar release (Fig. 6i). The low temperature portion of the release gives an age of 1.66 ± 0.05 Ga. This age may correspond to the age of an impact event in the vicinity of Luna 24 landing site, such as the Picard X crater. At higher temperatures apparent ages increase progressively to a maximum of 3.72 ± 0.01 Ga. This is considered to be the minimum age for crystallisation of the breccia.

In summary, the crystallisation ages obtained for basalt samples from the Luna 24 show a wide range between 2.52and 3.45 Ga suggesting a long period (0.9 Ga) of volcanism within the Crisium Basin occurring during several eruptive periods, as will be discussed later. It is interesting to note that four of the samples examined in this study 24077,92- D, 24109,92-E, 24210,60-C and 24210,60-B show recent impact events in the vicinity of the Luna 24 landing site at ~0.53, ~1.11, ~1.70 and ~1.84 Ga respectively.

3.4. Cosmic Ray Exposure (CRE) Ages

Determination of CRE ages of the individual fragments presents similar challenges due to the existence of cosmogenic, trapped and nucleogenic ^{38}Ar components, the latter being formed by neutron absorption by ^{37}Cl during the irradiation procedure. The presence of ^{37}Cl-derived ^{38}Ar is usually apparent in heating steps with $^{38}Ar/^{36}Ar$ ratios above the cosmogenic value of 1.54. Samples containing trapped and cosmogenic ^{38}Ar have $^{38}Ar/^{36}Ar$ values of between 0.187 and 1.54 respectively, CRE ages are best determined from $^{38}Ar/^{36}Ar$ vs. $^{37}Ar/^{36}Ar$ mixing diagrams (not shown) because Ca (monitored by $^{37}Ar_{Ca}$ during irradiation) is the dominant target element for cosmogenic ^{38}Ar in most lunar samples. CRE ages are summarised in Tables 2 and 3 and were calculated for the $^{38}Ar/^{37}Ar$ slope using a nominal ^{38}Ar production rate of 1.4×10^{-8} cm^3 g^{-1} Ca Ma^{-1} (Turner et al., 1971; Hennessy and Turner, 1980). The appropriate choice of production rate is somewhat arbitrary and uncertain unless the chemical composition of the sample is known. Hohenberg et al. (1978) estimate that production rates at between 0.8×10^{-8} and 1.2×10^{-8} cm^3 g^{-1} Ca Ma^{-1} as being appropriate for depths between 10 and ~150 g cm^{-2}, with the peak occurring at a depth of 50 g cm^{-2}. At depths $<$ 10 g cm^{-2} production rates rise rapidly due to production from solar flare.

The samples yield a wide span of CRE ages of 151-1280 Ma and 35-1642 Ma for Luna 16 and Luna 24 respectively. These CRE ages fall within the range previously reported for Luna samples (Huneke et al., 1972; Schaeffer et al., 1978; Stettler and Albarède, 1978; Wasserburg et al., 1978; Hennessy and Turner, 1980; Shanin et al., 1982; Burgess and Turner, 1998; Cohen et al., 2001). The wide range of CRE ages obtained for Luna 16 and Luna 24 regolith fragments is typical for the lunar regolith which is constantly stirred by burial and re-exposure to cosmic rays. However, it may have been expected that differences in CRE ages would be more evident corresponding to different depositional depths within the lunar regolith. One explanation for the lack of stratification in exposure ages is that the core-tubes in the Luna missions were not totally filled, and free space existed permitting the movement and mixing of the regolith particles within the tubes. Moreover, lunar regolith mixing models suggest that lunar fragments may have resided at different depths during their residence time near the lunar surface (Russ et al., 1972; Burnett and Woolum, 1974; Bogard and Hirsch, 1978; Nishiizumi and Imamura, 1979), and the actual CRE age determined may not be representative of a continuum lunar surface residence of the sample.

4. DISCUSSION

4.1. Mare Fecunditatis

The five Luna 16 basalt fragments used in the present study were either from the upper most layer of the core (21000) or

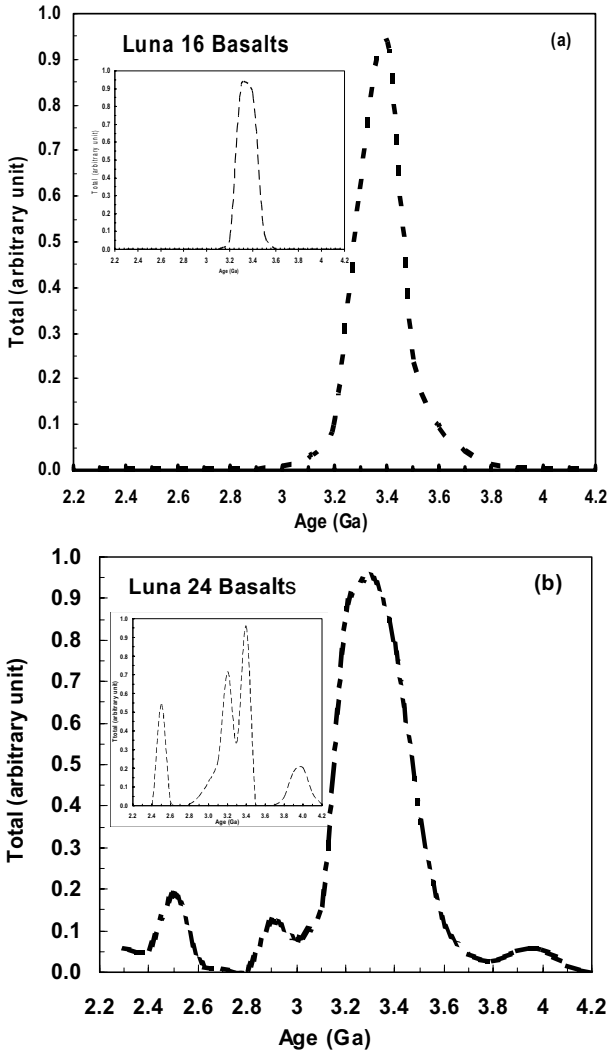

Fig. 7. Ideograms showing cumulative Ar-Ar age determinations for (a) Luna 16 and (b) Luna 24 samples. Data are from this study and literature sources (Cadogan and Turner, 1977; Huneke et al., 1978; Schaffer et al., 1978; Stettler and Albarède, 1978; Wasserburg et al., 1978; Hennessy and Turner, 1980; Shanin et al., 1982; Fugzan et al., 1986; Burgess and Turner, 1998; Cohen et al., 2001). Inserted figures show ideograms using only the results obtained from this study.

from shallow depths (21013). Their near-surface location accounts for their relatively high concentrations of trapped Ar. The age determinations obtained in this study are combined with those from previous studies (Cadogan and Turner, 1977; Huneke and Wasserburg, 1978; Cohen et al., 2001), to form the ideogram shown in Fig. 7a. This ideogram is based on a Gaussian curve calculation, which takes into account both the age and uncertainty of each sample. It should be noted that those samples containing high trapped Ar contents, and from which reliable ages could not be determined, were not considered in calculating the Gaussian curve. The ideogram shows a single age peak at ~3.35 Ga (Fig. 7a) indicating that the mare basalts sampled by Luna 16 were formed during a short period of volcanism within the Fecunditatis Basin. Based upon remote sensing data of Mare Fecunditatis there appear to be three main flows (Spudis and Pieters, 1991). The lava flow on which Luna 16 landed has an intermediate TiO_2 content (4.77%, Haskin and Warren, 1991) and appears to be younger than the other two larger flows. We tentatively suggest that the age of this flow is ~3.35 Ga. Two samples record the effects of local impact events that partially re-set the Ar systematics of the samples at ~1.64 Ga (21000,20-B) recording the age of an Eratosthenian crater (e.g. Langrenus crater, ~130 km in diameter and ~270 km south of Luna 16 landing site) and ~0.93 Ga (21013,51-B impact spherule) during formation of a crater of Copernican age (e.g. Taruntius crater, ~56 km in diameter and ~270 km north from Luna 16 landing site). The age of Taruntius had previously been suggested to be ~1.0 Ga (Spudis, 1989). CRE ages show a wide range of exposures reflecting the complex histories of individual lunar regolith fragments.

4.2. Mare Crisium

In the present study, we have determined the age of nine basaltic fragments from the Luna 24 landing site. The ages obtained are within those determined previously using ^{40}Ar-^{39}Ar and Sm-Nd analytical methods (Schaffer et al., 1978; Stettler and Albarède, 1978; Wasserburg et al., 1978; Hennessy and Turner, 1980; Shanin et al., 1982; Fugzan et al., 1986; Burgess and Turner, 1998; Cohen et al., 2001). Currently there are ages for 36 fragments and the cumulative data is shown as an ideogram in Fig. 7b. Sample 24077,92-B gave an age of 3.96 Ga within error of the age of Crisium Basin formation 3.89 ± 0.02 Ga ago (Podosek et al., 1973; Cadogan and Turner, 1977; Swindle et al., 1991; Stöffler and Ryder, 2001), and has a pyroxene composition that is distinct from other pyroxenes in Luna 24 basalts (Fig. 2). This sample is considered to be a more ancient basalt that was brecciated and underwent K/Ar age resetting during the Crisium impact, for this reason the age of this sample has not been included in the ideogram (Fig. 7b). In Figure 7b the curve for Luna 24 ages suggests the existence of more than one episode of lava extrusion, as well as for a protracted period of volcanism within the Crisium Basin. A dominant peak is for ages between 3.2 and 3.3 Ga with suggestions of younger lava flows occurring at ~3.0 and ~2.5 Ga. These results imply that Mare Crisium volcanism occurred over a long time period of 0.8 Ga. This period started in the Late Imbrium (the period when the majority of basalts were extruded; Wilhelms, 1987), some ~0.6 Ga after Crisium basin formation and continued into the Eratosthenian (Fig.7b).

Pieters and McCord (1976), Pieters (1978), Boyce et al. (1977), and especially Head et al. (1978) using remote sensing data together with laboratory data, suggested the existence of at least 4 different lava flows within Mare Crisium (see Fig. 10 of Head et al., 1978). The flow at the Luna 24 landing site corresponds to group IIA of Head et al. (1978) and is characterised as a ferrobasalt with very low TiO_2 content. The age of this unit may therefore correspond to the dominant peak at ~3.3 Ga (Fig. 7b; this study; Burgess and Turner, 1998; Cohen et al., 2001; Stöffler and Ryder, 2001). The two older basalt units IIB and I (Head et al., 1978) may therefore have erupted between 3.3 and 3.6 Ga (the oldest Luna 24 basalt age reported; Stettler and Albarède, 1978). The less well-defined, younger volcanism at 2.5 Ga may correspond to group III of Head et al. (1978).

Previously a protracted period of basalt extrusion within the

Crisium Basin (i.e. 2.30–3.60 Ga) was proposed (Boyce and Johnson, 1977, Shanin et al., 1982; Wilhelms 1987, Burgess and Turner, 1998). Wilhelms (1987) suggested that the emplacement of lava flows within a basin is most favoured by depressed elevations, and thin crust and lithosphere. Head and Wilson (1992) also suggested other factors that are important in the process of lava filling of the basins including: (1) magma buoyancy (see also Delano 1990; Hess and Parmentier, 1995; Wieczorek et al., 2001); (2) impact topography effects on the ascent of magma (causing fractures which subsequently provide pathways for magma forming sills and dykes); and (3) the thermal evolution trends, not only the localized magma melt due to the heat generated by the impact but also the weakening of the lithosphere diminishing the obstruction to the magma ascent.

Upon the formation of a basin due to an impact, up to tens of kilometers of crustal material (upper crust) are removed. Usually a partial refill of the basin with ejecta follows (Wilhelms, 1987), however, for the Crisium Basin this does not appear to have been the case. The noritic lower crust is exposed, which has a higher density (3100 kg/m^3; Wieczorek and Phillips, 1998) than most lunar basalts including the VLT Luna 24 samples (using the density of 2900 kg/m^3 of the model by Wieczorek et al., 2001). Thus, the buoyancy contrast between crust and uprising magma enables the eruption of basalts in Mare Crisium. The depression created on the crust is isostatically compensated by the uplift of the mantle, creating what is referred to as mascon (Muller and Sjörgen, 1968; Wilhelms, 1987). Mascons are usually formed by the combination of crustal thickness due to mantle uplift and the downward flexure of the lithosphere due to mare loading (Neumann et al., 1998). The volume of lava that fills the basins is most likely dependent on the magma-source production rate and depth (Hess and Parmentier, 1999; Hess, 2000; Head and Wilson, 1992; Wieczorek et al., 2001) and the thickness of the crust. It has been proposed that the crust within Mare Crisium is unusually thin, approaching ~0 km thickness (Zuber et al., 1994) and therefore not imposing any crustal obstruction for the ascent of mare basalts. The heating of the basalt source region may be related to the high heat production associated with the nearby Procellarum-KREEP Terrane (PKT) region (Haskin, 1998; Jolliff et al., 2000; Korotev et al., 2000). The high heat production of the PKT is probably responsible for the long duration of melting beneath that region of the Moon, and due to its proximity to Crisium, melting there might have been enhanced as well. In support of this, large impact basins on the farside, which are far from the PKT, contain a lesser amount of post-impact lava flows. There are also models proposed by Elkins-Tanton et al. (2004) suggesting that impact cratering itself might be the cause of melting beneath basins. However, this seems unlikely in light of the numerical simulations carried out by Ivanov and Melosh (2003), of the impact of an asteroid with a diameter of 20 km striking at 15 km s^{-1} into a target with a near-surface temperature gradient of 13 K km^{-1} ("cold" case) or 30 K km^{-1} ("hot" case). The modelled impact creates a 250- to 300-km-diameter crater and produced ~10,000 km^3 of impact melt. A crater collapse follows and the pressure field returns to near its initial lithostat. They concluded that even an impact of these dimensions couldn't raise mantle material above the peridotite solidus by decompression.

5. SUMMARY

Nineteen fragments from Luna 16, 20 and 24 regolith cores have been analysed by Ar-Ar laser probe. Trapped components dominated the Ar content of all three Luna 20 basalts such that it has not been possible to determine meaningful ages for these samples. Six Luna 16 give a dominant age of ~3.4 Ga in agreement with previous age determinations for this site. The ages of Luna 24 mare basalts span over a period of ~0.9 Ga suggesting a protracted period of volcanism in the Crisium basin. Most samples give an age of ~3.3 Ga, with a few younger basalts which crystallised at ~2.92 Ga, and the youngest at 2.5 Ga. These results extend previous studies based on other chronological work and underline the importance of combining age determinations and remote sensing data. The age of the lava flow upon which the Luna 24 mission landed (designated as group IIA by Head et al., 1978) possibly corresponds with the most common age of ~3.3 Ga. The long period of volcanism in the Crisium Basin may be due to formation of the basin by impact forming a thin crust with fracturing of the underlying lithosphere without substantial refill of the basin by ejecta. As a result of the impact and removal of crustal material, the mantle was uplifted and there was little crustal obstruction for the eruption of lava basalts. The Crisium Basin also borders the PKT region, potentially a long-lived heat-generating source in the lunar mantle.

Acknowledgments—We thank NASA for generously providing the Luna samples for this study. Dave Blagburn and Bev Clementson are thanked for technical support in the noble gas laboratory. We are grateful for the assistance of Steve Caldwell, Dave Plant and Chris Hayward during SEM and EMPA. We appreciate reviews from E. K. Jessberger and four anonymous reviewers which led to important for improvements of the manuscript. We also thank Mark Wieczorek for his valuable comments. Financial support was provided by an EEC-TMR fellowship and by a partial scholarship by Fundação para a Ciência e a Tecnologia of Portugal to VAF.

Associate editor: T. M. Harrison

REFERENCES

Albee A. L., Chodos A. A., Gancarz A. J., Haines E. L., Papanastassiou D. A., Ray L., Wasserburg G. J., and Wen T. (1972) kineralogy, petrology, and chemistry of a Luna 16 Basaltic Fragment, Sample B-1. *Earth Planet. Sci. Lett.* **13,** 353–367.

Bell J. F. and Hawke B. R. (1984) Lunar dark-haloed impact craters: Origin and implications for early mare volcanism. *J. Geophys. Res.* **103,** 6899–6970.

Bogard D. D. and Hirsch W. C. (1978) Noble gases in Luna 24 core soils. In *Mare Crisium: The View From Luna 24* (eds. R. B. Merrill and J. J. Papike), pp. 105–116. Pergamon Press, New York.

Borg L. E., Shearer C. K., Asmeron Y., and Papike J. J. (2004) Evidence for prolonged KREEP magmatism on the Moon from the youngest dated lunar igneous rock. *Nature* **432,** 209–211.

Boyce J. M. and Johnson D.A. (1977) Ages of flow units in Mare Crisium based on crater density. In *Proc. 8th Lunar Planet. Sci. Conf.*, pp. 3495–3502.

Boyce J. M., Schaber G. G., and Dial A. L. (1977) Age of Luna 24 mare basalts based on crater studies. *Nature* **265,** 38–39.

Burgess R. and Turner G. (1998) Laser ^{40}Ar-^{39}Ar age determinations of Luna 24 mare basalts. *Meteorit. Planet. Sci.* **33,** 921–935.

Burnett D. S. and Woolum D. S. (1974) Lunar neutron capture as a tracer for regolith dynamics. *Proc. 5th Lunar Sci. Conf.*, pp. 2061–2074.

Cadogan P. H. and Turner G. (1977) ^{40}Ar-^{39}Ar dating of Luna 16 and Luna 20 samples. *Philos. Trans. R. Soc. London, Ser. A* **284,** 167–177.

Cohen B. A., Snyder G. A., Hall C. M., Taylor L. A., and Nazarov M. A. (2001) Argon-40–argon-39 chronology and petrogenesis along the eastern limb of the Moon from Luna 16, 20 and 24 samples. *Meteorit. Planet. Sci.* **36,** 1345–1366.

Coish R. A. and Taylor L. A. (1978) Mineralogy and petrology of basaltic fragments from the Luna 24 drill core. In *Mare Crisium: The View From Luna 24* (eds. R. B. Merrill and J. J. Papike), pp. 403–418. Pergamon Press, New York.

Dalrymple G. B. (1991) *The Age of the Earth*. Stanford University Press, Stanford, CA.

Delano J. W. (1990) Buoyancy-driven melt segregation in the Earth's Moon, I. Numerical results. In *Proc. 20th Lunar Planet. Sci. Conf.*, pp. 3-12.

Elkins-Tanton L. T., Hager B. H., and Grove T. (2004) Magmatic effects of the lunar late heavy bombardment. *Earth Planet. Sci. Lett.* **222,** 17–27.

Fernandes V. A., Burgess R., and Turner G. (2000) Laser ^{40}Ar-^{39}Ar studies of Dar al Gani 262 lunar meteorite. *Meteorit. Planet. Sci.* **35,** 1355–1364.

Fernandes V. A., Burgess R., and Turner G. (2003) ^{40}Ar-^{39}Ar chronology of lunar meteorites Northwest Africa 032 and 773. *Meteorit. Planet. Sci.* **38,** 555–564.

Fugzan M. M., Gang V. M., Tarasov L. S., Kolesov G. M., and Shukolyukov Y. A. (1986) ^{40}Ar-^{39}Ar dating of lunar rocks from Mare Crisium. *Geokhimiya* **4,** 469–479.

Grieve R. A. F., McKay G., and Weill D. F. (1972) Microprobe studies of three Luna 16 basalt fragments. *Earth Planet. Sci. Lett.* **13,** 233–242.

Haskin L. A. (1998) The Imbrium impact event and the thorium distribution at the lunar highlands surface. *J. Geophys. Res.* **103,** 1679–1689.

Haskin L. and Warren P. (1991) Lunar chemistry. In *Lunar Source Book: A User's Guide to the Moon* (eds. G. H. Heiken, D. T. Vaniman and B. M. French), pp. 357–474. Cambridge University Press, Cambridge, UK.

Hawke B. R., Lucey P. G., Bell J. F., and Spudis P. D. (1990) Ancient mare volcanism. LPI-LAPST Workshop on Mare Volcanism and Basalt Petrogenesis: Astounding Fundamental Concepts (AFC) Developed Over the Last Fifteen Years. LPI Tech. Report. 91-03, pp. 5–6. Lunar Planetary Inst.

Head J. W. and Wilson L. (1992) Lunar mare volcanism: Stratigraphy, eruption conditions, and the evolution of secondary crusts. *Geochim. Cosmochim. Acta* **56,** 2155–2175.

Head J. W., Adams J. B., McCord T. B., Pieters C. M. and Zisk S. (1978) Regional stratigraphy and geologic history of Mare Crisium. In *Mare Crisium: The View From Luna 24* (eds. R. B. Merrill and J. J. Papike), pp. 43–74. Pergamon Press, New York.

Head J. W., Wilson L., and Wilhelms D. (1997) Lunar Mare basalt volcanism: Early stages and secondary crustal formation and implications for petrogenetic evolution and magma emplacement processes. *Lunar Planet. Sci. Conf.* **28,** abstract #1112.

Hennessy J. and Turner G. (1980) ^{40}Ar-^{39}Ar ages and irradiation history of Luna 24. *Philos. Trans. R. Soc. London, Ser. A* **297,** 27–39.

Hess P. C. (2000) On the source regions for mare picrite glasses. *J. Geophys. Res.* **105,** 4347–4360.

Hess P.C. and Parmentier E. M. (1995) A model for the thermal and chemical evolution of the Moon's interior: Implications for the onset of mare volcanism. *Earth Planet. Sci. Lett.* **134,** 501–514.

Hess P. C. and Parmentier E. M. (1999) Asymmetry and timing of mare volcanism. *Lunar Planet. Sci. Conf.* **30,** abstract #1300.

Hiesinger H. and Head J. W., III (2003) Ages and stratigraphy of mare basalts in Oceanus Procellarum, Mare Nubium, Mare Cognitum, and Mare Insularum. *J. Geophys. Res.* **108,** *E7*, 5065.

Hiesinger H., Jaumann R., Neukum G., and Head J. W. (2000) Ages of mare basalts on the lunar nearside. *J. Geophys. Res.* **105,** 29239–29275.

Hohenberg C. M., Marti K., Podosek F. A., Reedy R. C., and Shirck J. R. (1978) Comparisons between observed and predicted cosmogenic noble gases in lunar samples. *Proc. Lunar Planet. Sci. Conf.* **9,** 2311–2344.

Hollister L. S. and Kulick C. H. (1972) Luna 16 sample G36: Another crystalline product of an extremely mafic magma. *Earth Planet. Sci. Lett.* **13,** 312–315.

Huneke J. C. and Wasserburg G. J. (1978) Sliva iz piroga (plum out of the pie): K/Ar evidence from Luna 20 rocks for lunar differentiation prior to 4.51 AE ago. *Proc. Lunar Planet. Sci.* **9,** 598–600.

Huneke J. C., Podosek F. A., and Wasserburg G. J. (1972) Gas retention and cosmic-ray exposure ages of a fragment from Mare Fecunditatis. *Earth Planet. Sci. Lett.* **13,** 375–383.

Ivanov B. A. and Melosh H. J. (2003) Impacts do not initiate volcanic eruptions: Eruptions close to the crater. *Geology* **31,** 869–872.

Jolliff B. L., Gillis J. J., Haskin L. A., Korotev R. L., and Wieczorek M. A. (2000) Major lunar crustal terranes: Surface expressions and crust-mantle origins. *J. Geophys. Res.* **105,** 4197–4216.

Korotev R. L. (2000) The 'Great Lunar Hot Spot' and the composition and origin and origin of the Apollo mafic ('LKFM') impact-melt breccias. *J. Geophys. Res.* **105,** 4317–4345.

Laul J. C., Vaniman D. T. and Papike J. J. (1978) Chemistry, mineralogy and petrology of seven >1mm fragments from Mare Crisium. In *Mare Crisium: The View From Luna 24* (eds. R. B. Merrill and J. J. Papike), pp. 537–568, Pergamon Press, New York.

Lawrence D. J., Feldman W. C., Barraclough B. L., Binder A. B., Elphic R. C., Maurice S., and Thomsen D. R. (1998) Global elemental maps of the Moon: The Lunar Prospector gamma-ray spectrometer. *Science* **281,** 1484–1489.

Lawrence D. L, Feldman W. C., Barraclough B. L., Binder A. B., Elphic R. C., Maurice S., Miller M. C., and Prettyman T. H. (1999) Delineating the major KREEP-bearing terranes on the Moon with global measurements of absolute thorium abundances. *Lunar Planet. Sci. Conf.* **30,** abstract #2024.

Ma M.-S. and Schmitt A. (1979) Petrogenesis of Luna 16 aluminous mare basalts. *Geophys. Res. Lett.* **6,** 909–912.

McCauley J. F. and Scott D. H. (1972) The geologic setting of the Luna 16 landing site. *Earth Planet. Sci. Lett.* **13,** 225–232.

Muller P. M. and Sjörgen W. L. (1968) Mascons: Lunar mass concentrations. *Science* **161,** 680–684.

Neumann G. A., Lemoine F. G., Smith D. E., and Zuber M. T. (1998) Lunar basins: New evidence from gravity for impact-formed mascons. In *Workshop on New Views on the Moon: Integrated Remotely Sensed, Geophysical, and Sample Datasets* (eds. B. Joliff and G. Ryder). Lunar Planet. Inst., Houston, TX.

Nishiizumi K. and Imamura M. (1979) The extent of lunar regolith mixing. *Earth Planet. Sci. Lett.* **44,** 409–419.

Papike J. J. and Vaniman D. T. (1978) Luna 24 ferrobasalts and mare basalt suite: Comparative chemistry, mineralogy, and petrology. In *Mare Crisium: The View From Luna 24* (eds. R. B. Merrill and J. J. Papike), pp. 371–401. Pergamon Press, New York.

Papike J. J., Ryder G. and Shearer C. K. (1998) Lunar samples. In *Planetary Materials* (ed. J. J. Papike), pp. 5-2–5-234. Mineralogical Society of America, Washington, DC.

Pieters C. M. (1978) Mare basalt types on the front side of the Moon: A summary of spectral reflectance data. In *Proc. 9th Lunar Planet. Sci. Conf.*, pp. 2825–2849.

Pieters C. M. and McCord T. B. (1976) Characterization of lunar mare basalt types: I. A remote sensing study using reflection spectroscopy of surface soils In *Proc. 7th Lunar Sci. Conf.*, pp. 2677-2690.

Podosek F. A., Huneke J. C., Gancarz A. J., and Wasserburg G. J. (1973) The age and petrography of two Luna 20 fragments and inferences for widespread lunar metamorphism. *Geochim. Cosmochim. Acta* **37,** 887–904.

Roddick J. C. (1983) High precision intercalibration of ^{40}Ar-^{39}Ar standards. *Geochim. Cosmochim. Acta* **47,** 887–898.

Russ G. P., Burnett D. S., and Wasserburg G. J. (1972) Lunar neutron stratigraphy. *Earth Planet. Sci. Lett.* **15,** 172–186.

Ryder G., McSween H. Y., and Marvin U. B. (1977) Basalts from Mare Crisium. *Moon* **17,** 263–287.

Schaber G. (1973) Lava flows in Mare Imbrium: Geologic evolution from Apollo orbital photography. In *Proc. 4th Lunar Sci. Conf.*, pp. 73–92.

Schaeffer O. A., Bence A. E., Eichhorn G., Papike J. J., and Vaniman D. T. (1978) ^{39}Ar-^{40}Ar and petrologic study of Luna 24

samples 24077,13. In *Proc. 9th Lunar Planet. Sci. Conf.*, pp. 2363–2373.

Schultz P. H. and Spudis P. D. (1983) Beginning and end of lunar mare volcanism. *Nature* **302,** 233–236.

Shanin L. L., Arakelyants M. M., Bogatikov O. A., Ivanenko V. V., Pupyrev Y. G., Tarasov L. S., and Frikh-Khar D. I. (1982) ^{39}Ar-^{40}Ar dating of lunar soil from Sea of Crises. *Geochem. Int.* **7,** 26–37.

Snyder G. A., Taylor L. A., Patchen A., Nazarov M. A., and Semenova T. S. (1999) Volcanism at Mare Fecunditatis: Mineralogy and petrology of 'new' Luna 16 basalts. *Lunar Planet. Sci. Conf.* **30,** abstract #1494.

Spudis P. D. (1989) Young dark mantle deposits on the Moon. NASA TM 4210, pp. 406–407.

Spudis P. and Pieters C. (1991) Global and regional data about the Moon. In *Lunar Source Book: A User's Guide to the Moon* (eds. G. H. Heiken, D. T. Vaniman and B. M. French), pp. 595–632. Cambridge University Press, Cambridge, UK.

Steele I. M. and Smith J. V. (1972) Mineral and bulk compositions of three fragments from Luna 16. *Earth Planet. Sci. Lett.* **13,** 323–327.

Stettler A. and Albarède F. (1978) ^{39}Ar-^{40}Ar systematics of two millimetre rock fragments from mare Crisium. *Earth Planet. Sci. Lett.* **38,** 401–406.

Stöffler D. and Ryder G. (2001) Stratigraphy and isotope ages of lunar geologic units: Chronological standard for the inner solar system. In *Chronology and Evolution of Mars* (eds. R. Kallenbach, J. Geiss and W. K. Hartmann), pp. 13–58. Kluwer Academic, Dordrecht, the Netherlands.

Swindle T. D., Spudis P. D., Taylor G. J., Korotev R. L., Nichols R. H., Jr., and Pillinger C. T. (1991) Searching for Crisium Basin ejecta: Chemistry and ages of Luna 20 impact melts. In *Proc. 21st Lunar Planet. Sci. Conf.*, pp. 167–181.

Taylor G. J., Warren P., Ryder G., Delano J. and Lofgren G. (1991) Lunar Rocks. In *Lunar Source Book: A User's Guide to the Moon* (eds. G. H. Heiken, D. T. Vaniman and B. M. French), pp. 183–284, Cambridge University Press, Cambridge, UK.

Turner G. and Cadogan P. H. (1974) Possible effects of ^{39}Ar recoil in ^{40}Ar/^{39}Ar dating. In *Proc. 3rd Lunar Sci. Conf.*, pp. 1613–1622.

Turner G., Huneke J. C., Podosek F. A., and Wasserburg G. J. (1971) ^{40}Ar-^{39}Ar ages and cosmic ray exposure ages of Apollo 14 samples. *Earth Planet. Sci. Lett.* **12,** 19–35.

Vaniman D. T. and Papike J. J. (1977) Ferrobasalts from Mare Crisium: Luna 24. *Geophys. Res. Lett.* **4,** 497–500.

Vinogradov A. P. (1971) Preliminary data on lunar ground brought to Earth by automatic probe "Luna-16." In *Proc. 3rd Lunar Sci. Conf.*, pp. 1–16.

Vinogradov A. P. (1973) Preliminary data on lunar soil collected by the Luna 20 unmanned spacecraft. *Geochim. Cosmochim. Acta* **37,** 721–729.

Wasserburg G. J., Radicati di Brozolo F., Papanastassiou D. A., McCulloch M. T., Huneke J. C., Dymek R. F., DePaolo D. J., Chodos A. A., and Albee A. L. (1978) Petrology, chemistry, age and irradiation history of Luna 24 samples. In *Mare Crisium: The View From Luna 24* (eds. R. B. Merrill and J. J. Papike), pp. 105–116. Pergamon Press, New York.

Wieczorek M. A. and Phillips R. J. (1998) Potential anomalies on a sphere: Applications to the thickness of a crust. *J. Geophys. Res.* **103,** 1715–1724.

Wieczorek M. A. and Phillips R. J. (2000) The "Procellarum KREEP Terrane": Implications for mare volcanism and lunar evolution. *J. Geophys. Res.* **105,** 20417–20430.

Wieczorek M. A., Zuber M. T., and Phillips R. J. (2001) The role of magma buoyancy on the eruption of lunar basalts. *Earth Planet. Sci. Lett.* **185,** 71–83.

Wilhelms D. E. (1987) *The Geologic History of the Moon*. USGS Prof. Paper 1348.

Williamson J. H. (1968) Least-squares fitting of a straight line. *Can. J. Phys.* **46,** 1845–1846.

Zuber M. T., Smith D. E., Lemoine F. G., and Neumann G. A. (1994) The shape and internal structure of the Moon from the Clementine mission. *Science* **266,** 1839–1843.

ELECTRONIC ANNEX

Supplementary data associated with this article can be found in the online version at 10.1016/j.gca.2005.05.017.